IEEE Access
Multidisciplinary ⋮ Rapid Review ⋮ Open Access Journal

Received 21 December 2022, accepted 26 January 2023, date of publication 6 February 2023, date of current version 10 February 2023.

Digital Object Identifier 10.1109/ACCESS.2023.3242970

RESEARCH ARTICLE

Control Loop Stability Criterion and Interaction Law Analysis for Grid-Connected Inverter in Weak Grid

FANG LIU, (Senior Member, IEEE), LINFENG HU, GENGTAO YUAN, BO LIU, AND YUANYUAN BIAN

School of Electrical and Automation Engineering, Hefei University of Technology, Hefei 230000, China

Corresponding author: Fang Liu (fragcelau@hfut.edu.cn)

This work was supported in part by the National Natural Science Youth Foundation of China under Grant 51907044.

ABSTRACT The study of stability criterion and interaction analysis for grid-connected inverter under weak grid is of great value. The previous stability criterion combined current loop, phase-locked loop and other loops together, and used the same external interface to analyze the system stability. It is difficult to independently analyze the interaction among these loops and then design the control loop parameters under the conclusions of the stability analysis. Different from traditional stability criterion, this paper proposes control loop stability criterion for grid-connected inverter from the perspective of controller bandwidth overlap. Firstly, the system d-q overall small-signal model G0 considering phase-locked loop (PLL) of grid-connected inverter under weak grid is given and split into three multiplied independent parts: grid impedance, phase-locked loop and current controller. Then using the equivalent loop ratio expression obtained by combining PLL and grid impedance together and then divided by the current controller, the control loop stability criterion is proposed. The proposed stability criterion can not only maintain the independence of each single loop, but also can analyze the overall system stability. So, further analysis of the interaction law among the three parts under this control loop stability criterion is carried out by deducing the expression of the bandwidth ratio n of the PLL and current controller. And it is found that under the weak grid, the interaction between the links will be generated when the bandwidth ratio is greater than the threshold of n. This phenomenon can be represented by the overlapping area of amplitude-frequency curves in the bode diagram for G0. And the weaker the grid or the closer the bandwidth of PLL is to current controller, the larger the overlapping area of amplitude-frequency curves, and the more likely it is to lead the closed-loop gain to infinity. Furthermore, when the bandwidth of the current controller is fixed, the threshold of n varies in the regions of less than 1 as well as more than 1 with the change of the grid strength. Therefore, the system can remain stable no matter what the bandwidth ratio of the phase-locked loop to the current controller is greater or less than 1. Accuracy of the proposed control loop stability criterion and interaction analysis is verified through simulation and experimental results.

INDEX TERMS Weak grid, control loop stability criterion, interaction law, controller bandwidth, stability boundary.

I. INTRODUCTION

In recent years, with the energy crisis of traditional fossil energy sources, more and more renewable energy sources (RESs) are integrated into the power grid through power electronic interfaces with high penetration. Therefore, the stability of power systems with high penetration of power electronic grid-connected interfaces has gradually become an important issue, especially the stability and interaction of grid-connected converters under weak grid conditions [1], [2], [3].

There are many factors affecting the stability of grid-connected inverter systems under weak grid conditions, so, many stability criteria have been proposed for identifying

The associate editor coordinating the review of this manuscript and approving it for publication was Youngjin Kim.

system stability and analyzing the mechanism of system destabilization [4], [5]. The interaction between the inverters and the weak grid is complex, and various important factors are intertwined together, which will cause a negative impact on the stability of the grid-connected system [6], [7], [8].

Many scholars have proposed stability criteria for various types of grid-connected systems from different modeling perspectives, and various studies have been conducted on system stability and destabilization mechanisms based on the stability criteria. Among them, the modeling methods commonly used to analyze high-penetration RES integration power systems are impedance models [9], [10], [11], [12], [13], [14], [15], state space models [16], [17], [18], [19], [20], and s-domain models based on transfer functions [21], [22], [23], [24], [25], [26], [27]. Accordingly, there are many stability criteria for impedance models, including traditional impedance criteria based on *d-q* coordinates, generalized impedance criteria based on polar coordinates, and sequence impedance criteria based on positive and negative sequence models. RD Middlebrook proposed a small-signal model based on impedance modeling in the DC-DC converter system and gave a method for identifying the system stability for the first time. The converters are divided into source-load subsystems, and the entire system stability is analyzed under the premise of ensuring the stability of each subsystem. This method has been widely used in AC grid-connected systems as well. With the high penetration of RESs connected to the grid, the factors affecting system stability become more and more complex. For this reason, some researchers have proposed stability criteria that are more suitable for complex grid situations. In [11], the small-signal impedance models of the converter and the grid were established, and the generalized impedance of the converter and the grid was defined. Then a generalized impedance criterion was proposed, and the reasons for the decrease of the stability of the converter system under weak grid conditions were explained. In [12], the sequence impedance model of the grid-connected direct-drive wind turbine system in the static coordinate system was established, a RLC grid-connected stability criterion was proposed, and the oscillation frequency and damping of the system were quantitatively analyzed. This method can reflect the influence of the change rule of the internal oscillation mode on the overall stability of the system. In the impedance model, the grid-connected system and the power grid are independent from each other, and the parameters and structural changes of either part do not affect the other [28]. And the stability criterion based on the impedance model can analyze the influence and interaction of the internal control or component parameters on the system stability by drawing the impedance curves while changing the parameter values. The stability criterion based on the state-space model usually requires the establishment of the state-space equations for the whole system, and the system stability is then analyzed based on Lyapunov First Approximation method. In [16], the state space small-signal model of the photovoltaic grid-connected inverter system was established, and the discontinuous stable region characteristics of the grid-connected system under a wide voltage range were obtained by means of the eigenvalue analysis method. And from the perspective of participating factors, the interaction law of oscillation modes between phase-locked loop and current loop, and the ''borrowing'' damping phenomenon under the weak grid were elaborated. Using the stability criterion based on the state space model, the overall oscillation modes and changing law of its damping ratio under different grid strength can be completely analyzed, but the interaction phenomenon cannot be illustrated by analytical expression. In addition, many researchers have proposed the stability criteria for the s-domain model based on the transfer function [21], [22], [23], [24], [25], [26], [27]. In [23], the linearized transfer function model of the VSC grid-connected system was established, and the stability of the VSC system under PV control and PQ control was compared and analyzed. Based on that, an analytical criterion for system instability is proposed, the influence of the controller parameters on the system stability was also studied, and the instability mechanism of the grid-connected inverter system in the weak grid was revealed.

The stability criteria based on the above three modeling methods are mostly evolutionary forms based on the traditional stability criterion method, which can effectively identify the stability performance of the system. Many researchers have studied the influence of the interaction between inverters and weak power networks on system stability based on above stability criteria [15], [16], [17], [18], [19], [20], [21], [22], [23]. For example, in [13], based on the generalized impedance criterion, the interaction between the phase-locked loop and the DC voltage outer loop of the grid-connected converter under the weak grid was studied, and the influence of the controller parameters of the converter on such interaction as well as the overall stability of the system was revealed. In [17], the state space small-signal model of the VSC-HVDC system was established, and the effects of the short-circuit ratio (SCR) and phase-locked loop parameters on the stability of the system were discussed. The authors pointed out that when SCR is relatively low, especially less than 1.3, the system stability will be greatly weakened, and the phase-locked loop performance under low SCR will be relatively poor. In [21], the interaction between the phase-locked loop and the current loop was clarified by deriving the current loop transfer function model considering the grid strength and impact of the phase-locked loop. Also, the stability performance under weak grid was studied with the change of phase-locked loop parameters and grid strength, and finally a voltage feedforward method was proposed to solve the instability problem under weak grid.

These stability criteria and interaction analysis mentioned above often use source-load or other similar two subsystems modeling method. From the perspective of field application, it is necessary to put all the control loops together and use unified interface to identify the system instability by means

of impedance scanning. This has achieved great success in the renewable energy converters [29], [30]. However, it is hard to understand how each individual loop analytically play the role during the interaction with each other because there are no analytical and independent equations to express the stability relationship between individual part and the overall system. Furthermore, it is hard to use these methods to guide the design of controller parameters, bandwidth and analysis of interaction laws analytically.

In order to solve the problems, different from traditional impedance stability criterion, this paper proposes control loop stability criterion for grid-connected inverter from the perspective of independent controller bandwidth. Firstly, this paper divided the current open-loop transfer function G0 into three multiplied parts: grid impedance, phase-locked loop and current controller. And the equivalent loop ratio expression was obtained by combining the phase-locked loop and grid impedance together and then divided by the current controller. Accordingly, the grid-connected inverter control loop stability criterion was proposed based on Nyquist's theorem. Secondly, the interaction law between the three parts was analyzed using the loop ratio expression, and it is found that the system can remain stable no matter what the bandwidth ratio of the phase-locked loop to the current controller is greater or less than 1.

The innovative contribution of this paper is to separate each loop as an independent part, which can not only maintain the independence of each single loop, but also can analyze the overall stability. The interaction among these loops and control loop parameters can also be independently analyzed and designed while maintaining the whole system stability.

The rest of the paper is organized as follows: the topology and the small-signal modeling of grid-connected inverter are presented in Section II and III. The control loop stability criterion under weak grid conditions is proposed in Section IV. Analysis of the interaction law between weak grid and inverter is investigated in Section V. Simulations in MATLAB/Simulink and the experiment based on the hardware-in-the-loop (HIL)platform to verify the efficiency of the proposed criterion are presented in Section VI.

II. CONTROL AND MATHEMATICAL MODELLING OF THREE-PHASE GRID-CONNECTED INVERTER

A. TOPOLOGY AND CONTROL OF THREE-PHASE GRID-CONNECTED INVERTER

The main circuit topology and control structure of the three-phase grid-connected inverter are shown in Fig.1. The ideal DC power supply is connected to the three-phase AC power grid through the three-phase half-bridge circuit, L-filter and grid impedance. The grid-connected inverter system in Fig.1 adopts the closed-loop control of the inverter output current feedback under the single synchronous rotating d-q coordinate system. The output of the current loop obtains the drive signal through the d-q inverse transformation and SPWM link to control the grid-connected inverter. A single synchronous rotating d-q PLL is used to track the grid vector.

In Fig.1, $C_{\rm dc}$ is the DC bus capacitor. L is the filtering inductance of the filter. The grid impedance part includes the resistance component $R_{\rm grid}$ and the inductance component $L_{\rm grid}$. E is the three-phase grid voltage. $I_{\rm ga}$, $I_{\rm gb}$, and $I_{\rm gc}$ are the three-phase currents output by the grid-connected inverter, respectively. $I_{{\rm g}d}$ and $I_{{\rm g}q}$ are the d-q components of the output current of the grid-connected inverter, respectively. $U_{\rm c}$ is the output voltage of the inverter. U_{cd} and U_{cq} are the d-q components of the output voltage of the grid-connected inverter, respectively. ω_0 is the grid reference angular frequency. U_g is the voltage in the grid connected point. $U_{{\rm g}d}$ and $U_{{\rm g}q}$ are the d-q components of the voltage in the grid connected point, respectively.

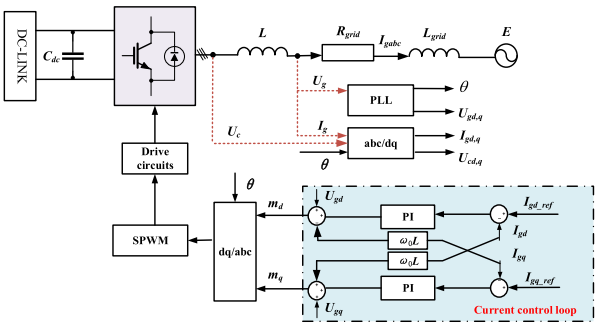

FIGURE 1. Grid-connected inverter and its control diagram.

Using the vector control in the d-q coordinate system, the voltage vector orientation standard is defined as follows: the orientation of the d-axis is fixed, the d-axis is 90° delayed of the q-axis, the angle between the PLL vector and the grid vector is δ. The vector diagram is shown in Fig. 2.

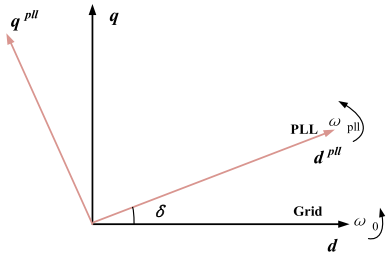

FIGURE 2. Phase relation between grid vector and PLL vector.

B. CURRENT LOOP MODEL

The control diagram of the current loop is shown in Fig. 3. The modulation signals m_d and m_q of the d- and q-axes are obtained through the closed-loop PI control link, the voltage feedforward link and the decoupling link of output current of inverter in the d-q coordinate system. Finally, the output voltages U_{cd} and U_{cq} of the grid-connected inverter are obtained through the SPWM link.

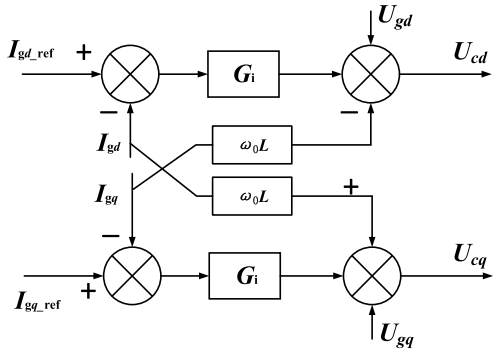

FIGURE 3. Control block diagram of current loop.

According to the control diagram of the current loop, the mathematical model can be obtained as:

$$\begin{cases} U_{cd} = G_i(I_{gd\_ref} - I_{gd}) - \omega_0 L I_{gq} + U_{gd} \\ U_{cq} = G_i(I_{gq\_ref} - I_{gq}) + \omega_0 L I_{gd} + U_{gq} \end{cases} \tag{1}$$

where

$$G_i = K_{p\_cl} + \frac{K_{i\_cl}}{s} \tag{2}$$

where $K_{\mathrm{p\_cl}}$ is the proportional coefficient of the PI controller for the current control loop. $K_{\mathrm{i\_cl}}$ is the integral coefficient of the PI controller for the current control loop. I_{gd_ref} is the reference value of the d-axis current of the current control loop. I_{gq_ref} is the reference value of the q-axis current of the current control loop. U_{gd} and U_{gq} are the d-q components of the voltage in the grid connected point, respectively. ω_0 is the grid reference angular frequency.

In order to improve the current following performance, the current regulator is designed according to the typical I type system [31], so the proportional coefficient and integral coefficient of the PI regulator for the current loop can be expressed as

$$\begin{cases} K_{p\_cl} = \omega_{CL} L \\ K_{i\_cl} = \omega_{CL} R_{grid} \end{cases} \tag{3}$$

where ω_{CL} is the control bandwidth of the current controller.

C. PLL MODEL

A single synchronous rotating d-q PLL is used to track the grid vector. According to the single synchronous rotating d-q PLL control algorithm, the control diagram of the PLL can be obtained as shown in Fig. 4.

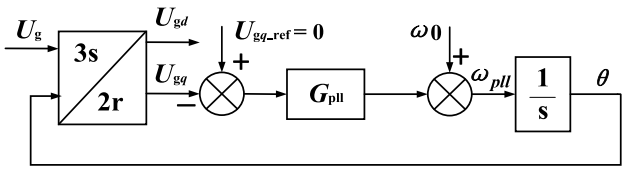

FIGURE 4. PLL control block diagram.

According to the PLL control diagram shown in Fig. 4, the mathematical model can be obtained as follows:

$$\begin{cases} \omega_{pll} = G_{pll}(0 - u_{gq}) + \omega_0 \\ \theta = s\omega_{pll} \end{cases} \tag{4}$$

where

$$G_{pll} = K_{p\_pll} + \frac{K_{i\_pll}}{s} \tag{5}$$

where ω_{pll} is the grid voltage angular frequency obtained from the PLL. $K_{\mathrm{p\_pll}}$ is the proportional coefficient of the PI controller for the PLL. $K_{\mathrm{i\_pll}}$ is the integral coefficient of the PI controller for the PLL. θ is the grid vector obtained from the PLL. ω_0 is the grid reference angular frequency.

The PLL is usually designed as a typical II type system [31], so the proportional and integral coefficients of the PI regulator for the PLL can be expressed as:

$$\begin{cases} K_{p\_pll} = \dfrac{2\zeta\omega_{PLL}}{U_{gd}} \\ K_{i\_pll} = \dfrac{2\zeta}{\omega_{PLL}} \end{cases} \tag{6}$$

where ω_{PLL} is the control bandwidth of the PLL, and ζ is the damping ratio of the PLL.

D. MAIN CIRCUIT MODEL

According to the topology of the grid-connected inverter shown in Fig. 1, the differential equations of the main circuit mathematical model is expressed in the d-q coordinate system and the s-domain as follows:

$$\begin{cases} sLI_{gd} = -R_{grid} I_{gd} + \omega_0 L I_{gq} + U_{cd} - U_{gd} \\ sLI_{gq} = -R_{grid} I_{gq} - \omega_0 L I_{gd} + U_{cq} - U_{gq} \end{cases}$$
$$\begin{cases} sL_{grid} I_{gd} = -R_{grid} I_{gd} + \omega_0 L_{grid} I_{gq} + U_{gd} - E_d \\ sL_{grid} I_{gq} = -R_{grid} I_{gq} - \omega_0 L_{grid} I_{gd} + U_{gq} - E_q \end{cases} \tag{7}$$

where s is the Laplace operator. E_d and E_q are the components on the d- and q-axes of the three-phase grid voltage, respectively.

Similarly, according to the topology of the grid-connected inverter shown in Fig. 1 and the vector relationship shown in Fig.2, the mathematical model of the grid in the d-q coordinate system can be obtained:

$$\begin{cases} E_d = U_{\mathrm{magg}} \cos\delta \\ E_q = -U_{\mathrm{magg}} \sin\delta \end{cases} \tag{8}$$

where U_{magg} is the peak value of grid phase voltage.

In addition, the SCR of the grid-connected inverter system refers to the ratio of the power grid short-circuit capacity S_{grid} to the inverter capacity S_{inv}:

$$SCR = \frac{S_{grid}}{S_{inv}} = \frac{U_{p-p}^2}{|Z| \times S_{inv}} \tag{9}$$

where $U_{\mathrm{p-p}}$ is phase-to-phase RMS voltage of the AC power grid; $|Z|$ is the amplitude of grid equivalent impedance, and $Z = R_{\mathrm{grid}} + \mathrm{j}\omega_0 L_{\mathrm{grid}}$. According to IEEE Standard

1204-1997 [32], the AC power grid with SCR < 3 is the weak power grid, and the power grid with SCR < 2 is the extremely weak power grid. This study is mainly aimed at the stability of grid-connected inverter systems under weak grid and extremely weak grid.

III. SMALL-SIGNAL MODEL

In order to further study the stability of the grid-connected inverter system, the entire system needs to be linearized. Based on equations (1)∼(8), the linearized small-signal model can be obtained through substituting all variables x with small disturbance form $x_0 + \Delta x$ and eliminating the steady-state variable in the equations, where x_0 represents the steady-state value of the variable, and Δx represents the small disturbance value of the variable. In addition, in order to emphasize the influence of the grid-connected inverter control loop on the system stability under weak grid, based on the linearized model from equations (1)∼(8), the current closed-loop transfer function considering the influence of power grid strength and PLL can be obtained as shown in [25]:

$$\begin{cases} \Delta I_{gd} = \dfrac{G_i}{G^*}\left[\dfrac{1-G_1}{1+G_0}\Delta I_{gd\_ref} - \dfrac{G_2}{1+G_0}\Delta I_{gq\_ref}\right] \\ \Delta I_{gq} = \dfrac{G_i}{G^*}\left[\dfrac{G_3}{1+G_0}\Delta I_{gd\_ref} + \dfrac{G_4}{1+G_0}\Delta I_{gq\_ref}\right] \end{cases} \tag{10}$$

where

$$\begin{cases} G^* = G_i + sL + R_{grid} \\ G_0 = \dfrac{G_i}{G^*}G_{PLL}[\omega_0 L_{grid} I_{gq0} - (sL_{grid} + R_{grid})I_{gd0}] \\ G_1 = \dfrac{G_i}{G^*}G_{PLL}(sL_{grid} + R_{grid})I_{gd0} \\ G_2 = \dfrac{G_i}{G^*}G_{PLL}(sL_{grid} + R_{grid})I_{gq0} \\ G_3 = \dfrac{G_i}{G^*}G_{PLL}\omega_0 L_{grid} I_{gd0} \\ G_4 = \dfrac{G_i}{G^*}G_{PLL}\omega_0 L_{grid} I_{gq0} \\ G_{PLL} = \dfrac{2\zeta\omega_{PLL}s + \omega_{PLL}^2}{U_{gd0}(s^2 + 2\zeta\omega_{PLL}s + \omega_{PLL}^2)} \end{cases} \tag{11}$$

Also, from equations (10)∼(11), the current loop control diagram can be obtained as follows:

Taking the d-axis current control loop as an example, ΔI_{gd_ref} and ΔI_{gd} are the input and output of the current loop respective, ΔI_{gq_ref} is the disturbance. The characteristic equation of the current loop can be obtained as $1+G_0$ according to equation (10) and the current loop control diagram in Fig.5. Based on automatic control principle [33], the open-loop transfer function G_0 can be used to identify the system stability in the followings.

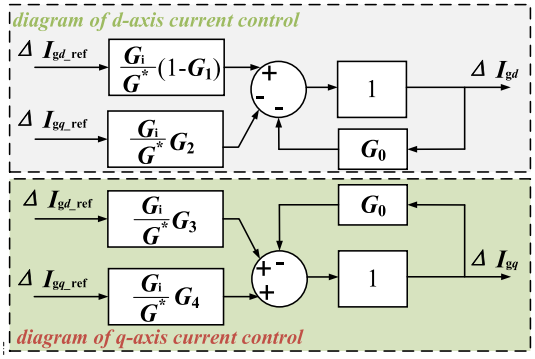

FIGURE 5. Current loop control block diagram considering PLL and power grid strength.

In this study, taking the system operation point in unit power factor an example, so, $I_{gq0} = 0$, the open-loop transfer function G_0 can be obtained as +:

$$\begin{aligned} G_0 &= -\frac{G_i}{G^*}G_{PLL}(sL_{grid} + R_{grid})I_{gd0} \\ &= -\frac{I_{gd0}}{U_{gd0}}\left[(sL_{grid} + R_{grid})\frac{\omega_{CL}}{s+\omega_{CL}}\frac{2\zeta\omega_{PLL}s + \omega_{PLL}^2}{s^2 + 2\zeta\omega_{PLL}s + \omega_{PLL}^2}\right] \end{aligned} \tag{12}$$

IV. THE STABILITY CRITERION OF GRID-CONNECTED INVERTER CONTROL LOOP UNDER WEAK GRID

It's not difficult to find that the open-loop transfer function G_0 is mainly composed of three multiplied parts from equation (12). Part I is the grid impedance, Part II is the current controller and Part III is the PLL. Their expressions are $G_{grid} = -\left(I_{gd0}/U_{gd0}\right)\left(sL_{grid} + R_{grid}\right)$, $G_{i\_close} = \omega_{CL}/(s+\omega_{CL})$ and $G_{pll\_close} = \left(2\zeta\omega_{PLL}s + \omega_{PLL}^2\right)/\left(s^2 + 2\zeta\omega_{PLL}s + \omega_{PLL}^2\right)$ respectively, which characterize the influence of grid strength, control bandwidth of current controller and the bandwidth of PLL on the stability of the grid-connected inverter system.

To further study the stability performance of the grid-connected inverter system under weak grid and the influence of the interaction between the control loops on the system stability, this paper proposes a control loop stability criterion by analogy with the Nyquist criterion [28].

Firstly, the PLL is closely related to the grid impedance part as tracking the voltage in the grid-connected point. For analysis, their influence on the stability of the grid-connected inverter can be regarded as one, that is, part I and part III can be regarded as a whole, which is denoted as $G_{\text{pll\_grid}}$,

$$\begin{aligned} G_{pll\_grid} &= G_{grid}G_{pll\_close} \\ &= -\frac{I_{gd0}}{U_{gd0}}\left[(sL_{grid} + R_{grid})\frac{2\zeta\omega_{PLL}s + \omega_{PLL}^2}{s^2 + 2\zeta\omega_{PLL}s + \omega_{PLL}^2}\right] \end{aligned} \tag{13}$$

A further identical transformation of the open-loop transfer function G_0 can be given as

$$G_0 = G_{pll\_grid} G_{i\_close} = \frac{G_n}{G_d} = \frac{G_{pll\_grid}}{1/G_{i\_close}} \tag{14}$$

Finally, the control loop stability criterion is given according to the generalized Nyquist criterion [33], where both amplitude and phase conditions need to be satisfied for the grid-connected inverter to be able to operate stably.

1) when $\angle G_{\rm n}$-$\angle G_{\rm d} = 180°$, $|G_{\rm d}\ (j\omega_{180°})| > |G_{\rm n}(j\omega_{180°})|$;

2) when $|G_{\rm d}| = |G_{\rm n}|$, $\angle G_{\rm n}(j\omega_{\rm inter})$-$\angle G_{\rm d}(j\omega_{\rm inter}) > -180°$;

Where $\omega_{180°}$ is the angular frequency corresponding to the point $\angle G_{\rm n}$ and $\angle G_{\rm d}$ differ by exactly 180°, and $\omega_{\rm c}$ is the angular frequency corresponding to the point $|G_{\rm d}|$ and $|G_{\rm n}|$ are exactly equal.

At the same time, the expressions for the amplitude margin and phase margin of the grid-connected inverter system can be given as

$$\begin{cases} A_M = \left|G_d(j\omega_{\rm g})\right| - \left|G_n(j\omega_g)\right| \\ \psi_M = 180^\circ + [\angle G_n(j\omega_{inter}) - \angle G_d(j\omega_{inter})] \end{cases} \tag{15}$$

According to the control loop stability criterion, when $\angle G_{\rm n}$-$\angle G_{\rm d} = 180°$, that is, at phase cross-over frequency $\omega_{180°}$ of the phase- frequency curve, the open-loop transfer function G_0 can satisfy the amplitude stability condition $|G_{\rm d}(j\omega_{180°})| > |G_{\rm n}(j\omega_{180°})|$. Further analysis indicate that the amplitude and phase of the open-loop transfer function G_0 can satisfy the stability condition to keep the closed-loop system stable when $|G_{\rm d}| > |G_{\rm n}|$ in the full band range.

It can be found that the maximum value of $|G_0|$ is approximately at the point $\omega \approx \omega_{\rm PLL}$ according the amplitude-frequency asymptote curve obtained from the open-loop transfer function G_0. Therefore, ensuring $20{\rm Lg}|G_0|_{\max} < 0$ can ensure that $|G_{\rm d}| > |G_{\rm n}|$ in the full range, that is

$$\begin{aligned} 20Lg\left|G_d(j\omega_{PLL})\right| &> 20Lg\left|G_n(j\omega_{PLL})\right| \\ \Leftrightarrow 20Lg\frac{\left|G_n(j\omega_{PLL})\right|}{\left|G_d(j\omega_{PLL})\right|} &< 0 \Rightarrow \frac{\left|G_n(j\omega_{PLL})\right|}{\left|G_d(j\omega_{PLL})\right|} < 1 \end{aligned} \tag{16}$$

From equation (16), it can be further derived that

$$\begin{aligned} &\frac{\left|G_n\left(j\omega_{PLL}\right)\right|}{\left|G_d\left(j\omega_{PLL}\right)\right|} \\ &= \frac{I_{gd0}\sqrt{\left(\omega_{PLL}L_{grid}\right)^2 + \left(R_{grid}\right)^2}\sqrt{1+(\frac{2\zeta\omega_{PLL}}{\omega_{PLL}})^2}}{U_{gd0}\sqrt{1+\frac{\omega_{PLL}^2}{\omega_{CL}^2}}\sqrt{(\frac{2\zeta\omega_{PLL}}{\omega_{PLL}})^2 + \left(1-\frac{\omega_{PLL}^2}{\omega_{PLL}^2}\right)^2}} < 1 \\ &= \left(\frac{I_{gd0}}{U_{gd0}}\sqrt{1+\frac{1}{4\xi^2}}\right) \times \frac{\sqrt{R_{grid}^2 + \left(\omega_{PLL}L_{grid}\right)^2}}{\sqrt{1+\left(\frac{\omega_{PLL}}{\omega_{CL}}\right)^2}} < 1 \end{aligned} \tag{17}$$

The identical transformation of equation (17) can be given as

$$\frac{R_{grid}^2 + \left(\omega_{PLL}L_{grid}\right)^2}{1+\left(\frac{\omega_{PLL}}{\omega_{CL}}\right)^2} < \left(\frac{U_{gd0}}{I_{gd0}\sqrt{1+\frac{1}{4\xi^2}}}\right)^2 \tag{18}$$

Observed from equation (18), it can be found that when the system is in the steady-state, the right side of the inequality is a fixed value, which is only related to the steady-state value of the output voltage and current of the grid-connected inverter, and is independent of the grid strength and the bandwidth of the controller, so this fixed value is denoted as A. Thus,

$$\frac{R_{grid}^2 + \left(\omega_{PLL}L_{grid}\right)^2}{1+\left(\frac{\omega_{PLL}}{\omega_{CL}}\right)^2} < A \tag{19}$$

To further investigate the restrictive relationship between the control bandwidth of the PLL $\omega_{\rm PLL}$ and the current controller $\omega_{\rm CL}$, substituting $\omega_{\rm PLL} = n\omega_{\rm CL}$ $(n > 0)$ into equation (19), it can be derived as

$$n^2 < \frac{A - R_{grid}^2}{L_{grid}^2\omega_{CL}^2 - A} \Leftrightarrow 0 < n < \sqrt{\frac{A - R_{grid}^2}{L_{grid}^2\omega_{CL}^2 - A}} \tag{20}$$

Similarly, if $\omega_{\rm CL} = m\omega_{\rm PLL}$ $(m > 0)$ is substituted into equation (19) it can be derived as

$$\begin{aligned} m^2 &< \frac{A}{R_{grid}^2 + \omega_{PLL}^2L_{grid}^2 - A} \\ &\Leftrightarrow 0 < m < \sqrt{\frac{A}{R_{grid}^2 + \omega_{PLL}^2L_{grid}^2 - A}} \end{aligned} \tag{21}$$

where $R_{\rm grid}$ and $L_{\rm grid}$ have a high value under weak grid, and the bandwidth of controller is not chosen to be too small, so the denominator on the right hand side of the inequality in both equation (20) and equation (21) is greater than zero, that is, the inequality is always meaningful.

In summary, a restrictive relationship between the control bandwidth of the PLL $\omega_{\rm PLL}$ and the current controller $\omega_{\rm CL}$ can be derived as shown in equations (20) and (21). Under weak grid, when one bandwidth of the controller is determined, another bandwidth of controller that satisfies the control loop stability criterion can be calculated. In this way, the instability problem of grid-connected inverter caused by control loops interaction under weak grid can be solved effectively.

V. INTERACTION ANALYSIS OF GRID-CONNECTED INVERTER SYSTEM UNDER WEAK GRID CONDITIONS

It can be seen that the closed-loop system can remain stable when the open-loop transfer function G_0 satisfies the control loop stability criterion given in Section IV. This section will analyze the interaction law of the grid-connected inverter system under weak grid conditions The parameters of the three-phase grid-connected inverter in this study are shown in Tab.1.

TABLE 1. Parameters of three-phase grid-connected inverter system.

Parameters	Value
Inductance (L)	2 mH
Swithcing frequency (f_{sw})	10 kHz
DC side voltage (U_{dc})	750 V
Base angular frequency (ω_0)	314.16 rad/s
Rated power (S_{base})	30 kVA
Rated current (I_{gd0})	45 A
Rated voltage (U_{gd0})	220 V
Damping ratio of PLL (ζ)	0.707
Base impedance (L_{grid},R_{grid})(SCR=1)	15.32H,0.48Ω

A. ANALYSIS OF INTERACTION LAW BETWEEN THE INVERTER SYSTEM AND THE WEAK GRID UNDER WEAK GRID CONDITIONS

When the systems with power electronic grid-connected interfaces are connected to the power grid with a high penetration, the grid equivalent impedance will become large, and the power grid will gradually be weaker. It can be obtained from equation (13) that the amplitude expression of the transfer function G_n related to the grid strength in the frequency domain can be expressed as

$$\begin{aligned}\left|G_{pll\_grid}\right| &= |G_n| \\ &= \frac{I_{gd0}\sqrt{R_{grid}^2+\left(\omega L_{grid}\right)^2}\sqrt{1+\left(\frac{2\xi}{\omega_{PLL}}\times\omega\right)^2}}{U_{gd0}\left(\frac{2\xi}{\omega_{PLL}}\times\omega\right)^2+\left(1-\frac{\omega^2}{\omega_{PLL}^2}\right)^2}\end{aligned} \tag{22}$$

It can be obtained from equation (22) that when the SCR gradually decreases, that is, the resistance component R_{grid} and the inductance component L_{grid} of the grid impedance gradually increase, the amplitude $|G_n(\omega)|$ of the G_n will also increase. This makes the amplitude condition of the control loop stability criterion '$|G_d(j\omega_{180°})| > |G_n(j\omega_{180°})|$' difficult to be satisfied, which will make the system develop towards the trend of instability. The interaction law between the inverter and the weak grid is shown in Fig. 6.

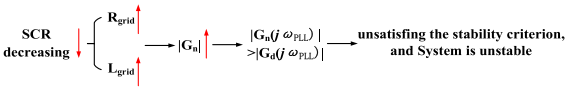

FIGURE 6. Interaction law between inverter system and weak grid.

The Bode plots and Nyquist curves of the open-loop transfer function G_0 under three weak grid conditions (SCR = 2.5, 1.5 and1.1, respectively) are shown in Fig.7 with $\omega_{CL} = 2\pi\times750$rad/s and $\omega_{PLL} = 2\pi\times50$rad/s.

It can be seen from Fig.7(a), when the bandwidths of the PLL and the current controller maintain constant, the grid-connected inverter system exhibits different stability performance under different weak grid conditions. The weaker the grid strength, the larger the amplitude $|G_n(\omega)|$, which makes $|G_n(\omega)|$ shift upward in the amplitude-frequency curve. It makes the amplitude-frequency curves of $|G_n(\omega)|$ and $|G_d(\omega)|$ gradually generate intersection point, and the overlapping area gradually becomes larger, that is, it is more and more difficult to satisfy the control loop stability criterion '$|G_d(j\omega_{180°})| > |G_n(j\omega_{180°})|$ for the amplitude condition, which will make the system stability deteriorate or even become unstable. Similarly, it can be seen from the Nyquist curves in Fig.7(b) that, the Nyquist curves of the G_0 do not encloses the point (−1, j0) counterclockwise when SCR = 2.5 and 1.5, respectively, therefore the system can remain stable. However, when SCR = 1.1, the Nyquist curve of the G_0 encloses the point (−1, j0) counterclockwise, which makes the system unstable, which is basically consistent with the Bode diagram analysis results.

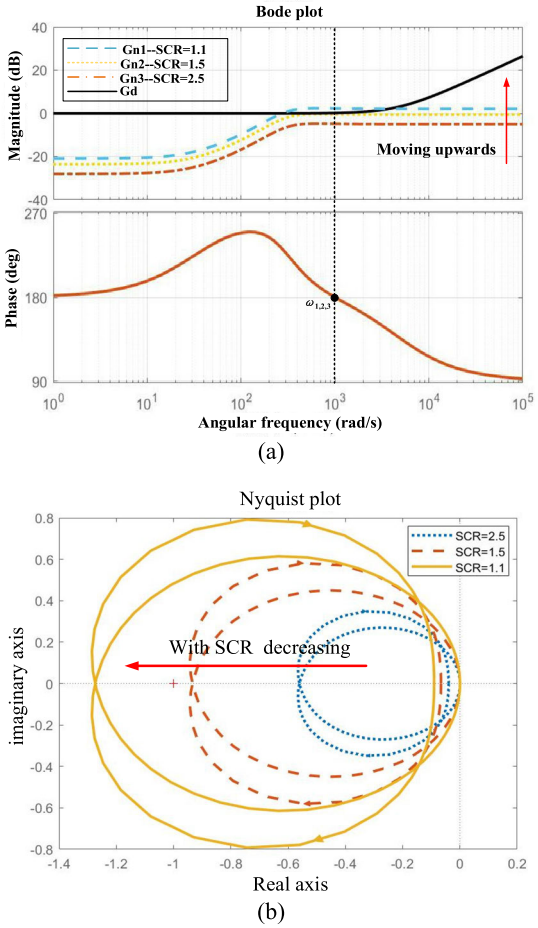

FIGURE 7. Bode plots and Nyquist curves of G0 under different SCR conditions((a) bode plot of G_0 for different SCR conditions, (b) Nyquist plot of G_0 for different SCR conditions).

According to the restrictive relationship between the control bandwidths of the PLL ω_{PLL} and the current controller ω_{CL} given by equation (19), when $\omega_{CL} = 2\pi\times150$rad/s, the value range of the bandwidth ratio n between the two controllers satisfying the control loop stability criterion under different SCR conditions is shown in Fig.8:

It can be seen from Fig.8 that under weak grid conditions, as the SCR gradually decreases, the ratio n also decreases gradually, and the corresponding stability range of the system

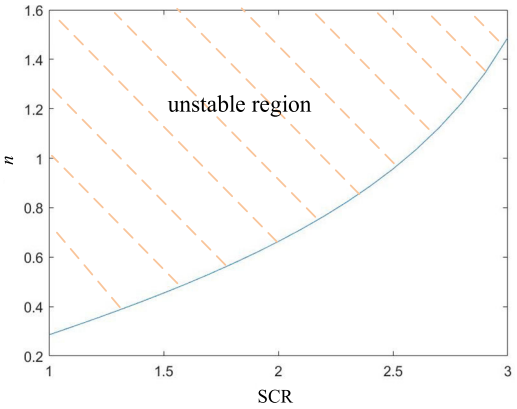

FIGURE 8. Value range of bandwidth ratio *n* under different SCR conditions.

is also gradually shrinking, that is, the stability of the system is gradually getting worse. However, it is worth noticing there exit some cases that the ratio n is greater than 1 in the stability range. It indicates that the grid-connected inverter system can also remain stable when the control bandwidth of the PLL ω_{PLL} is larger than the bandwidth of the current controller ω_{CL}. The restrictive relationship between the bandwidths of the PLL and the current controller changes with different grid strengths, thus the variation law of the stability range of the grid-connected inverter system with the decreasing SCR is shown from a quantitative perspective.

B. ANALYSIS OF INTERACTION LAW BETWEEN CONTROL LOOP BANDWIDTHS OF GRID-CONNECTED INVERTER SYSTEM

In order to further analyze the influence of the control bandwidths of the current controller and the PLL on the stability of the grid-connected inverter system and the law of interaction between them. According to the analysis results in Section IV, it is necessary to ensure that $|G_{\mathrm{d}}(\omega)|$ is greater than $|G_{\mathrm{n}}(\omega)|$ as far as possible in the full frequency range.

In the frequency domain, the amplitude expression $|G_{\mathrm{d}}(\omega)|$ of G_{d} can be obtained as:

$$|G_d(\omega)| = \sqrt{1 + \frac{\omega^2}{\omega_{CL}^2}} \tag{23}$$

It can be seen from equations (22) and (23) that $|G_{\mathrm{d}}(\omega)|$ is mainly related to the bandwidth of the current controller ω_{CL} and its value decreases with the increase of ω_{CL}. $|G_{\mathrm{n}}(\omega)|$ is mainly related to the grid strength (L_{grid}, R_{grid}) and the control bandwidth of the PLL ω_{PLL}, and its value increases with the decrease of grid strength or the increase of ω_{PLL}. Considering both the Bode plot and the Nyquist curve, the geometric explanation is further given as follows:

Case 1: Given SCR = 1.5, $\omega_{\mathrm{CL}} = 2\pi \times 750$rad/s. Based on equation (19), the value range of the control bandwidth of the PLL that satisfies the control loop stability criterion can be calculated as: $\omega_{\mathrm{PLL}} \leq 0.08\omega_{\mathrm{CL}} = 2\pi \times 60$rad/s. When $\omega_{\mathrm{PLL}} = 2\pi \times 30$rad/s, $2\pi \times 80$rad/s and $2\pi \times 130$rad/s, respectively, the Bode plots and Nyquist curves corresponding open-loop transfer function G_0 are shown in Fig.9 and Fig.10.

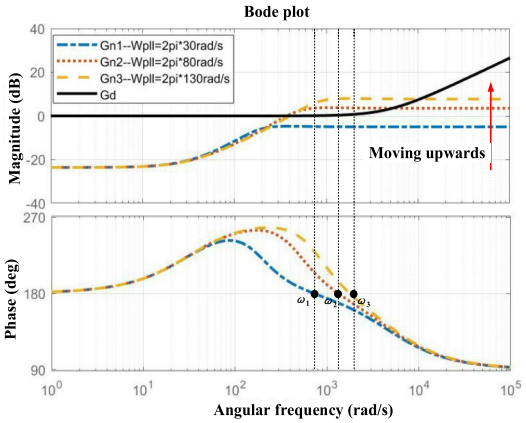

FIGURE 9. Bode diagram of open loop transfer function G_0 in case 1.

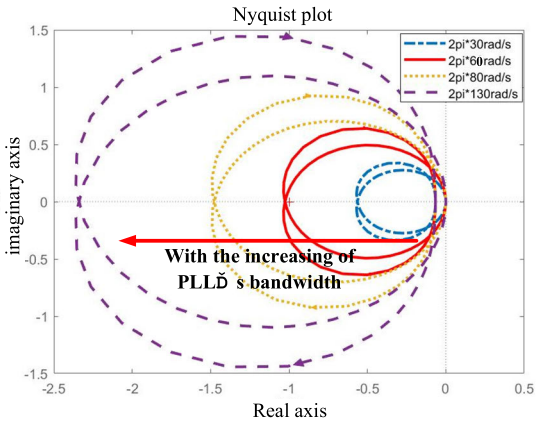

FIGURE 10. Nyquist curve of open loop transfer function G_0 in case 1.

It can be seen from Fig.9 that when $\omega_{\mathrm{PLL}} = 2\pi \times 30$rad/s, $|G_{\mathrm{d}}(\omega_1)| > |G_{\mathrm{n}}(\omega_1)|$ at the phase cross-over frequency ω_1 of the system, which satisfies the control loop stability criterion. However, under the condition that the strength of the power grid and the bandwidth of the current controller maintain constant, increasing the control bandwidth of the PLL will make $|G_{\mathrm{n}}(\omega)|$ increase, which is represented as an upward shift of $|G_{\mathrm{n}}(\omega)|$ in the amplitude-frequency curve. It will make the two amplitude-frequency curves gradually generate an intersection point, and the overlapping area will gradually become larger. At the same time, the amplitude condition '$|G_{\mathrm{d}}(j\omega_{180^\circ})| > |G_{\mathrm{n}}(j\omega_{180^\circ})|$' of the control loop stability criterion is difficult to be satisfied, which will make the system develop towards the trend of instability. Therefore, when the bandwidth of the current controller is determined under weak grid conditions, in order to avoid the interaction between the PLL and the current loop, the bandwidth of the PLL should be limited to a reasonable range, so that the amplitude-frequency curves of transfer function $G_{\mathrm{n}}(\omega)$ and $G_{\mathrm{d}}(\omega)$ do not intersect. Similarly, from the Nyquist curve

given in Fig.10, it can also be found that when the value of ω_{PLL} gradually decrease, the Nyquist curve of G_0 gradually encloses the point $(-1, \mathrm{j}0)$ counterclockwise, and the Nyquist curve of G_0 exactly encloses the point $(-1, \mathrm{j}0)$ counterclockwise when the threshold is chosen for the control bandwidth ω_{PLL}, which is consistent with the analysis conclusion of the Bode plot.

Case 2: Given SCR $= 1.5$, $\omega_{\mathrm{PLL}} = 2\pi \times 65$rad/s. Based on equation (19), the value range of the bandwidth of the current controller that satisfies the control loop stability criterion can be calculated as: $\omega_{\mathrm{CL}} \leq 3.2\omega_{\mathrm{PLL}} = 2\pi \times 210$rad/s. When $\omega_{\mathrm{PLL}} = 2\pi \times 50$rad/s, $2\pi \times 250$rad/s and $2\pi \times 450$rad/s, respectively, the Bode plots and Nyquist curves of the open-loop transfer function G_0 are shown in Fig.11 and Fig.12.

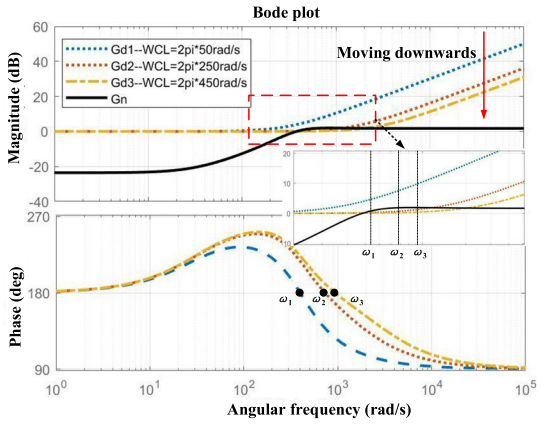

FIGURE 11. Bode diagram of open loop transfer function G_0 in case 2.

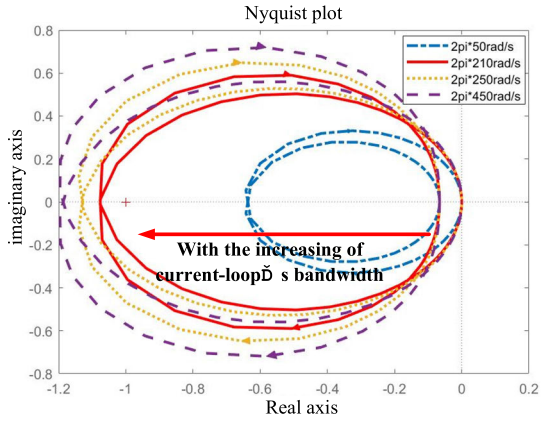

FIGURE 12. Nyquist curve of open loop transfer function G_0 in case 2.

It can be seen from Fig.11 that when $\omega_{\mathrm{CL}} = 2\pi \times 50$rad/s, $|G_{\mathrm{d}}(\omega_1)| > |G_{\mathrm{n}}(\omega_1)|$ at the phase cross-over frequency ω_1 of the system, which satisfies the control loop stability criterion. However, under the condition that the strength of the power grid and the bandwidth of the PLL maintain constant, increasing the control bandwidth of the current controller will make $|G_{\mathrm{d}}(\omega)|$ decrease, which is represented as a downward shift of $|G_{\mathrm{d}}(\omega)|$ in the amplitude-frequency curve. It will make the two amplitude-frequency curves gradually generate an intersection point, and the overlapping area will gradually become larger. Meanwhile, the amplitude condition '$|G_{\mathrm{d}}(j\omega_{180^\circ})| > |G_{\mathrm{n}}(j\omega_{180^\circ})|$' of the control loop stability criterion is difficult to be satisfied, which will make the system develop towards the trend of instability. Therefore, when the bandwidth of the PLL is determined under weak grid conditions, in order to avoid the interaction between the PLL and the current loop, the bandwidth of the current controller should be limited to a reasonable range, so that the amplitude-frequency curves of the $G_{\mathrm{n}}(\omega)$ and $G_{\mathrm{d}}(\omega)$ do not intersect. Similarly, from the Nyquist curve given in Fig.12, it can also be observed that when the value of ω_{CL} gradually increase, the Nyquist curve of G_0 gradually encloses the point $(-1, \mathrm{j}0)$ counterclockwise, and the Nyquist curve of G_0 exactly encloses the point $(-1, \mathrm{j}0)$ counterclockwise when the threshold is chosen for the control bandwidth ω_{CL}, which is consistent with the analysis result of the Bode plot.

Through the above analysis, it can be concluded that under some weak grid conditions, the control bandwidths of the current loop and PLL must satisfy the restrictive relationship defined in equation (20), so that the grid-connected inverter system can operate stably. That is, once one bandwidth of the controller is determined, then the stable boundary of the bandwidth corresponding another controller can be calculated. Fig.13 shows the stability boundaries of the control bandwidths under different weak grid conditions (SCR $= 1 \sim 3$).

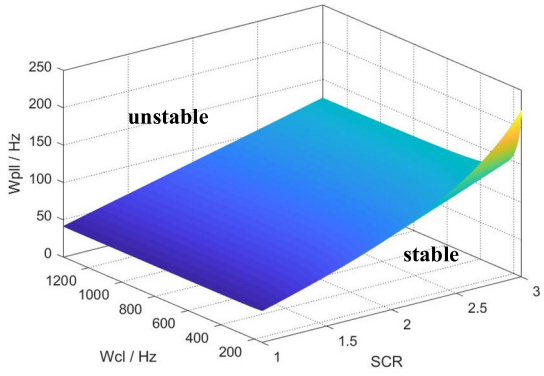

FIGURE 13. The controller bandwidth stability boundary under different SCR conditions.

It can be clearly seen from Fig.13 that under different weak grid conditions, both controllers have their own stability ranges. The stability ranges can be calculated from equation (20), and the reasonable design of the controller bandwidths can effectively avoid the instability caused by the interaction between control loops under weak grid conditions.

Based on the analysis in Sections V-A and V-B, it can be concluded that under weak grid conditions, the interactions of the grid-connected inverter system can easily lead to system instability. There are two reasons. One reason is the interaction between the power grid and the inverter system. The greater the amplitude of grid equivalent impedance

(the weaker the power grid), the greater the influence of the interaction, and the more likely the system will be unstable. The second reason is the interaction between the control loop bandwidths, which is shown in the Bode plot as an overlap between the amplitude curves of the two control loops.

VI. SIMULATIONS AND EXPERIMENTATION

In order to verify the correctness of interaction law of the grid-connected inverter system analyzed in Section V Based on Fig.1, a simulation model of the three-phase grid-connected inverter is built in MATLAB/Simulink for verification, and the experimental verification is carried out in the hardware-in-the-loop simulation platform.

A. SIMULATIONS RESULTS

In this section, the simulation verification results in MATLAB/Simulink will be presented. The three-phase grid-connected inverter capacity is 30kVA, and the specific parameters of the system are consistent with Tab.1.

1) SIMULATION VERIFICATION OF THE INTERACTION LAW BETWEEN THE GRID-CONNECTED INVERTER SYSTEM AND THE WEAK GRID

The same parameters as Section V-A are used in Simulink for verification, where $\omega_{CL} = 2\pi \times 750$rad/s, $\omega_{PLL} = 2\pi \times 50$rad/s, and SCR $= 2.5$, 1.5 and 1.1 respectively. The output current waveforms of the grid-connected inverter under different SCR conditions are shown in Fig.14.

Under the same set of controller parameters, when the SCR $= 2.5$ and 1.5 respectively, the output current of the grid-connected inverter is stable as shown in Fig.14(a) and 14(b). When SCR $= 1.1$, the output current of the grid-connected inverter oscillates and the system is unstable as shown in Fig.14(c). The threshold of SCR to stabilize the system is approximately 1.3 shown in Section V-A, so the simulation results are consistent with the analysis results in Section V-A.

In addition, when $\omega_{CL} = 2\pi \times 150$rad/s, $\omega_{PLL} = 2\pi \times 164$rad/s, the output current waveform of the grid-connected inverter under weak grid condition (SCR $= 3$) is shown in Fig.15. It can be seen from Fig.15, the output current of the grid-connected inverter in this case is stable, which is consistent with the analysis results in Section V-A.

2) SIMULATION VERIFICATION OF THE INTERACTION LAW OF THE CONTROL LOOPS IN THE GRID-CONNECTED INVERTER SYSTEM

In order to verify the interaction law between the control loops of the grid-connected inverter under the weak grid conditions given in Section V-B, this section compares the stability performance of the grid-connected inverter system when different values are chosen for the control bandwidths of the PLL and the current controller under different weak grid conditions.

Tab.2 gives the theoretical calculation threshold bandwidths of the PLL corresponding to different bandwidths of the current controllers in different scenarios. In Scenario I and Scenario II, the SCR $= 2$, the $\omega_{CL} = 100$Hz

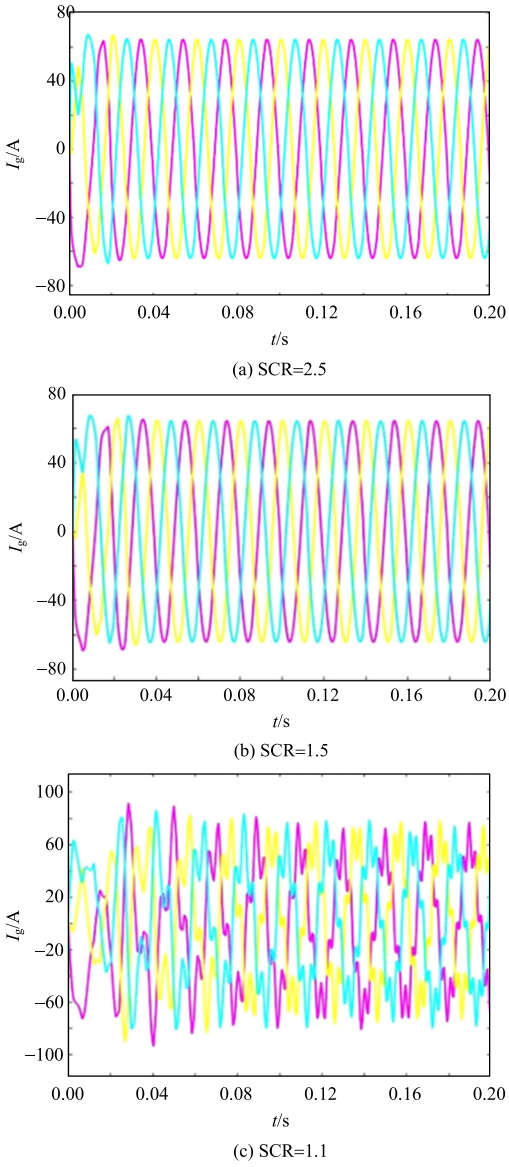

FIGURE 14. Current of grid-connected inverter under different SCR conditions.

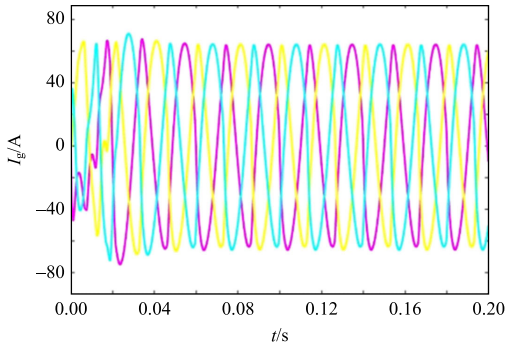

FIGURE 15. When the phase-locked loop is larger than the current loop bandwidth, the grid-connected inverter outputs the current waveform.

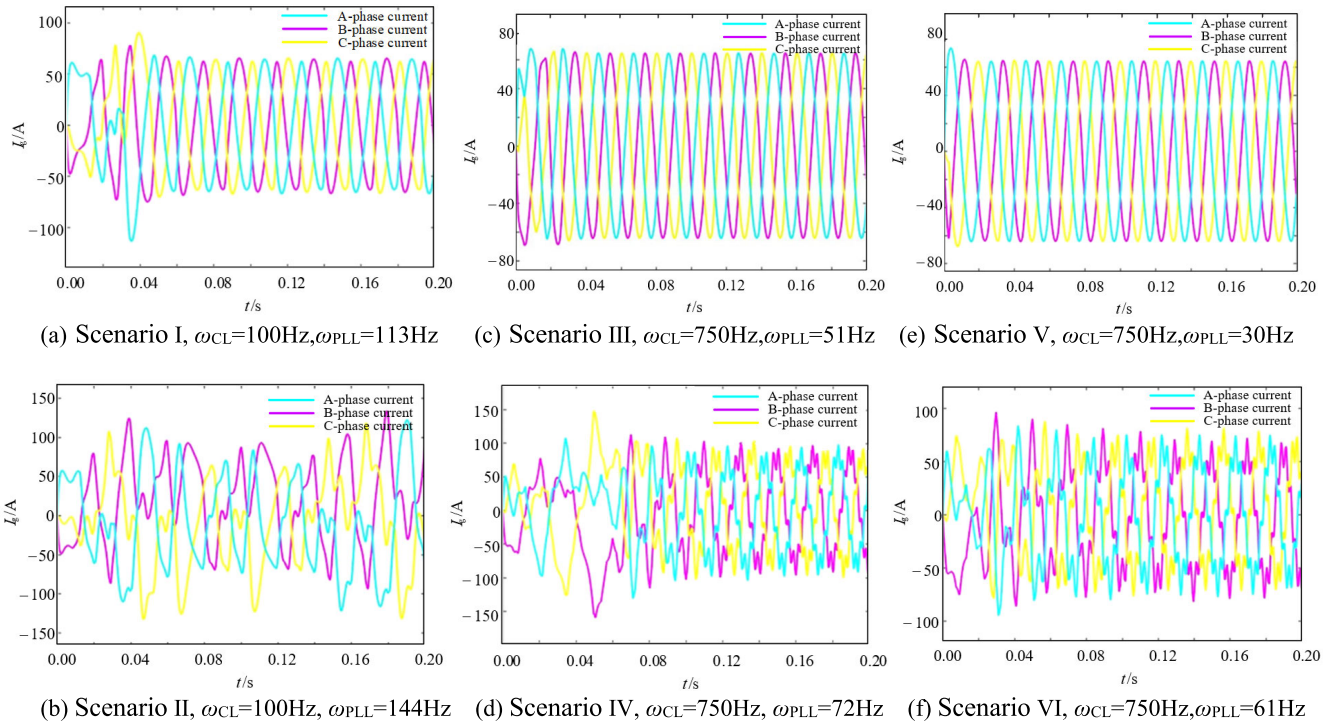

(a) Scenario I, ω_{CL}=100Hz,ω_{PLL}=113Hz (c) Scenario III, ω_{CL}=750Hz,ω_{PLL}=51Hz (e) Scenario V, ω_{CL}=750Hz,ω_{PLL}=30Hz

(b) Scenario II, ω_{CL}=100Hz, ω_{PLL}=144Hz (d) Scenario IV, ω_{CL}=750Hz, ω_{PLL}=72Hz (f) Scenario VI, ω_{CL}=750Hz,ω_{PLL}=61Hz

FIGURE 16. Current of grid-connected inverter under different SCR and different control bandwidth.

TABLE 2. Control loop's bandwidth in myltiple situations.

Situation	SCR	ω_{CL}(Hz)	Threshold of ω_{PLL}(Hz)	ω_{PLL}(Hz)
I	2	100	142	113
II	2	100	142	144
III	1.5	750	60	51
IV	1.5	750	60	72
V	1.2	750	49	30
VI	1.2	750	49	61

(corresponding the threshold control bandwidth of the PLL to stabilize the system is 142Hz), and the $\omega_{PLL} = 113$Hz and 144Hz, respectively. In Scenario III and Scenario IV, the SCR = 1.5, the $\omega_{CL} = 750$Hz (corresponding the threshold control bandwidth of the PLL to stabilize the system is 60Hz), and the $\omega_{PLL} = 51$Hz and 72Hz, respectively. In addition, for Scenario V and Scenario VI, the SCR = 1.2, the $\omega_{CL} = 750$Hz (corresponding the threshold control bandwidth of the PLL to stabilize the system is 49Hz), and the $\omega_{PLL} = 30$Hz and 61Hz, respectively.

From the output current waveforms of the grid-connected inverters in the six different scenarios shown in Fig. 16, it can be seen that under weak grid conditions, when the bandwidth of the current controller is determined, as long as the bandwidth of the PLL does not exceed the threshold, even if the control bandwidth of the PLL is greater than the bandwidth of the current controller, the output current waveforms of the grid-connected inverter can still remain stable. However, once the threshold is exceeded, the output current waveforms of the grid-connected inverter will oscillate and the system will be unstable. This is consistent with the analysis results given in Section V-B.

B. EXPERIMENTAL RESULTS

In order to further verify the theoretical analysis of the interaction law of grid-connected inverters under weak grid conditions, the hardware-in-the-loop experiment platform is built as shown in Fig. 17, and the capacity of the three-phase grid-connected inverter is 30kVA. DSP TMS320F28335 is used for control algorithm, and the specific experimental parameters are the same as those in Tab.1.

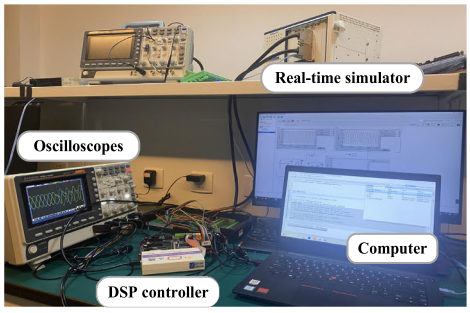

FIGURE 17. Hardware-in-the-loop experimental platform.

1) EXPERIMENTAL VERIFICATION OF THE INTERACTION LAW BETWEEN THE GRID-CONNECTED INVERTER SYSTEM AND THE WEAK GRID

The same parameters as in Section V-A are used in the experiments for verification. When SCR = 2.5, 1.5 and 1.1 respectively, the output current waveforms of the grid-connected inverters under different weak grid conditions are shown in Fig. 18.

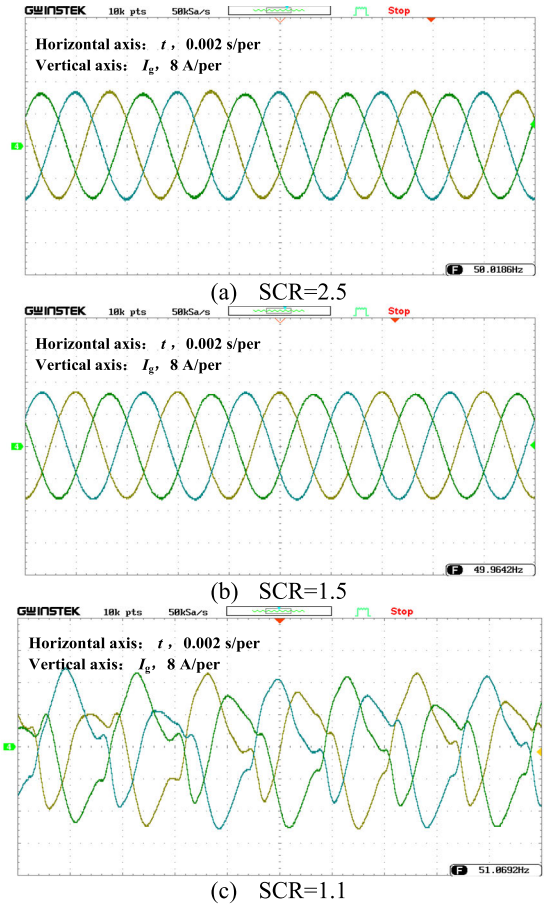

FIGURE 18. Current of grid-connected inverter under different SCR conditions.

It can be seen from Fig. 18 that under the same set of controller parameters, when the SCR = 2.5 and 1.5, respectively, the output current of the grid-connected inverter is stable as shown in Fig.18(a) and 18(b). When SCR = 1.1, the output current of the grid-connected inverter oscillates, and the system is unstable as shown in Fig. 18(c). This is consistent with the simulation results and the theoretical analysis results in Section VI-A and Section V-A

2) EXPERIMENTAL VERIFICATION OF THE INTERACTION LAW OF THE CONTROL LOOPS IN THE GRID-CONNECTED INVERTER SYSTEM

The same parameters as in Section V-A are used in the experiments for verification in Section VI-A. The output

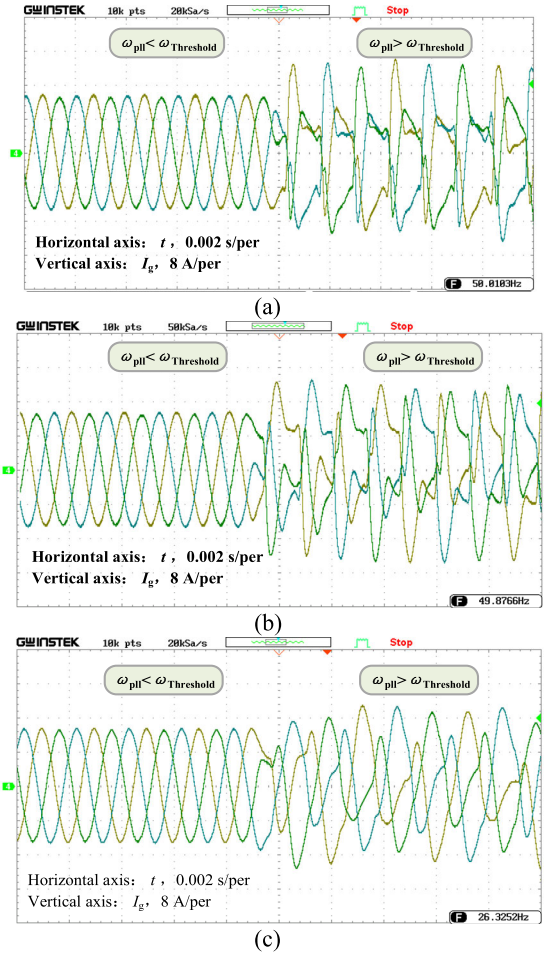

FIGURE 19. Current of grid-connected inverter under different SCR and different control bandwidth((a) Situation I, SCR = 2, (b) Situation II, SCR = 1.5, (c) Situation III, SCR = 1.1).

current waveforms of the grid-connected inverters are shown in Fig. 19.

As can be seen from Fig.19, when the bandwidth of the current controller is determined, if the control bandwidth of the PLL is smaller than the threshold, the output current waveform of the grid-connected inverter is stable. However, once the threshold is exceeded, the output current waveform of the grid-connected inverter is prone to oscillation and the system is unstable. The experimental results are consistent with the simulation results and the theoretical analysis results in Section VI-A and Section V-B.

VII. CONCLUSION

In this paper, based on the three-phase grid-connected inverter topology, a current closed-loop transfer function considering the influence of grid strength and PLL is derived, and a control loop stability criterion under weak grid conditions is proposed. Based on the stability criterion, the interaction law of the grid-connected inverter system under weak grid conditions is analyzed. The main conclusions are as follows:

1) The control loop stability criterion is proposed based on Nyquist's theory. This method can separate each loop as an independent object during the process of building the system model, which can not only reflect the independence of the control loop, but also can analyze the overall stability from the perspective of the system. The interaction among these loops and control loop parameters can also be independently analyzed and designed while maintaining the system stability.

2) Under weak grid conditions, the interaction between the inverter and the weak grid will make the stability boundary of the control loop shrink, and the weaker the grid, the greater the influence of the interaction. The restrictive relationship between the control bandwidth of the PLL and the current controller changes with the grid strength, and the system can still remain stable even when the bandwidth of PLL is larger than the current controller

3) Under weak grid conditions, the interaction among the control loops of the grid-connected inverter can lead to system instability, and the weaker the grid or the closer the bandwidth of PLL is to current controller, the greater the influence of the interaction. Under different weak grid conditions, the bandwidth of the PLL and the current controller have their own stability ranges. By calculating the range of the stability region, the reasonable design of the controller bandwidth can effectively avoid the instability caused by the interaction between control loops under weak grid conditions.

This paper takes the d-axis current control as an example, and does not study the q-axis current control. In the future work, the q-axis current control will be studied, and the same and different points of d-axis and q-axis current control will be analyzed.

REFERENCES

[1] D. Zhu, S. Zhou, X. Zou, and Y. Kang, "Improved design of PLL controller for LCL-type grid-connected converter in weak grid," *IEEE Trans. Power Electron.*, vol. 35, no. 5, pp. 4715–4727, May 2020.

[2] G. Wu, H. Sun, X. Zhang, A. Egea-Alvarez, B. Zhao, S. Xu, S. Wang, and X. Zhou, "Parameter design oriented analysis of the current control stability of the weak-grid-tied VSC," *IEEE Trans. Power Del.*, vol. 36, no. 3, pp. 1458–1470, Jun. 2021.

[3] M. Li, X. Zhang, Z. Guo, H. Pan, M. Ma, and W. Zhao, "Impedance adaptive dual-mode control of grid-connected inverters with large fluctuation of SCR and its stability analysis based on D-partition method," *IEEE Trans. Power Electron.*, vol. 36, no. 12, pp. 14420–14435, Dec. 2021.

[4] S. Silwal, S. Taghizadeh, M. Karimi-Ghartemani, M. J. Hossain, and M. Davari, "An enhanced control system for single-phase inverters interfaced with weak and distorted grids," *IEEE Trans. Power Electron.*, vol. 34, no. 12, pp. 12538–12551, Dec. 2019.

[5] M. Amin and M. Molinas, "Understanding the origin of oscillatory phenomena observed between wind farms and HVDC systems," *IEEE J. Emerg. Sel. Topics Power Electron.*, vol. 5, no. 1, pp. 378–392, Mar. 2017.

[6] M. Li, X. Zhang, Z. Guo, J. Wang, Y. Wang, F. Li, and W. Zhao, "The control strategy for the grid-connected inverter through impedance reshaping in Q-axis and its stability analysis under a weak grid," *IEEE J. Emerg. Sel. Topics Power Electron.*, vol. 9, no. 3, pp. 3229–3242, Jun. 2021.

[7] K. Sun, W. Yao, J. Fang, X. Ai, J. Wen, and S. Cheng, "Impedance modeling and stability analysis of grid-connected DFIG-based wind farm with a VSC-HVDC," *IEEE J. Emerg. Sel. Topics Power Electron.*, vol. 8, no. 2, pp. 1375–1390, Jun. 2020.

[8] G. Wu, "Analysis and design of vector control for VSC-HVDC connected to weak grids," *CSEE J. Power Energy Syst.*, vol. 3, no. 2, pp. 115–124, Jun. 2017.

[9] W. Wu, "Sequence impedance modeling and stability comparative analysis of voltage-controlled VSGs and current-controlled VSGs," *IEEE Trans. Power Electron.*, vol. 66, no. 8, pp. 6460–6472, Aug. 2019.

[10] Z. Zeng, H. Xiao, C. Niu, J. Chen, Z. Wang, X. Wu, and M. Cheng, "An improved impedance modeling method of grid-tied inverters with white-box property," *IEEE Trans. Power Electron.*, vol. 37, no. 4, pp. 3980–3989, Apr. 2022.

[11] H. Xin, Z. Li, and W. Dong, "Generalized-impedance and stability criterion for grid-connected converters," *Proc. CSEE*, vol. 37, no. 5, pp. 1277–1293, 2017.

[12] H. Zhang, Z. Li, and X. Shen, "Research on RLC stability criterion of sequence-impedance-model-based direct driven wind-turbine generator grid-connected system," *Hubei Electr. Power*, vol. 43, no. 6, pp. 78–85, 2019.

[13] C. Yang, Z. Gong, and M. Hong, "Applicability analysis of the generalized-impedance stability criterion for converters considering the outer-loop dynamics," *Proc. CSEE*, vol. 41, no. 9, pp. 3012–3024, 2021.

[14] B. Wen, D. Boroyevich, R. Burgos, P. Mattavelli, and Z. Shen, "Analysis of D-Q small-signal impedance of grid-tied inverters," *IEEE Trans. Power Electron.*, vol. 31, no. 1, pp. 675–687, Jan. 2016.

[15] Y. Qi, P. Lin, Y. Wang, and Y. Tang, "Two-dimensional impedance-shaping control with enhanced harmonic power sharing for inverter-based microgrids," *IEEE Trans. Power Electron.*, vol. 34, no. 11, pp. 11407–11418, Nov. 2019.

[16] F. Liu, W. Liu, and S. Liu, "Small Signal modeling and discontinuous stability regions analysis of grid-connected inverters considering control delay in wide range grid," *Acta Engergie Solaris Sinica*, vol. 43, no. 1, pp. 418–428, 2022.

[17] Z. Jenny, "Impact of short circuit ratio and phase locked loop parameters on the small-signal behaviour of a VSC-HVdc converter," in *Proc. IEEE Power Energy Soc. Gen. Meeting (PESGM)*, Jul. 2016, p. 1.

[18] Y. Wang, X. Wang, F. Blaabjerg, and Z. Chen, "Harmonic instability assessment using state-space modeling and participation analysis in inverter-fed power systems," *IEEE Trans. Ind. Electron.*, vol. 64, no. 1, pp. 806–816, Jan. 2017.

[19] M. Rasheduzzaman, J. A. Mueller, and J. W. Kimball, "An accurate small-signal model of inverter-dominated islanded microgrids using *DQ* reference frame," *IEEE J. Emerg. Sel. Topics Power Electron.*, vol. 2, no. 4, pp. 1070–1080, Dec. 2014.

[20] Y. Wang, X. Wang, F. Blaabjerg, and Z. Chen, "Harmonic instability assessment using state-space modeling and participation analysis in inverter-fed power systems," *IEEE Trans. Ind. Electron.*, vol. 64, no. 1, pp. 806–816, Jan. 2017.

[21] Z. Xie, Y. Chen, W. Wu, W. Gong, and J. M. Guerrero, "Stability enhancing voltage feed-forward inverter control method to reduce the effects of phase-locked loop and grid impedance," *IEEE J. Emerg. Sel. Topics Power Electron.*, vol. 9, no. 3, pp. 3000–3009, Jun. 2021.

[22] Z. Shuai, Y. Li, W. Wu, C. Tu, A. Luo, and J. Z. Shen, "Divided DQ small-signal model: A new perspective for the stability analysis of three-phase grid-tied inverters," *IEEE Trans. Ind. Electron.*, vol. 66, no. 8, pp. 6493–6504, Aug. 2019.

[23] B. Shao, S. Zhao, and B. F. Gao, "Instability mechanism and criterion analysis of VSC-HVDC connected to the weak AC power grid," *Trans. China Electrotech. Soc.*, vol. 34, no. 18, pp. 3884–3896, 2019.

[24] M. F. M. Arani and Y. A.-R. I. Mohamed, "Analysis and performance enhancement of vector-controlled VSC in HVDC links connected to very weak grids," *IEEE Trans. Power Syst.*, vol. 32, no. 1, pp. 684–693, Jan. 2017.

[25] G. Wu, X. Zhou, and S. Wang, "Analytical research on the mechanism of the interaction between PLL and inner current loop when VSC-HVDC connected to weak grid," *Proc. CSEE*, vol. 38, no. 9, pp. 2622–2633, 2018.

[26] Y. Huang, X. Yuan, J. Hu, and P. Zhou, "Modeling of VSC connected to weak grid for stability analysis of DC-link voltage control," *IEEE J. Emerg. Sel. Topics Power Electron.*, vol. 3, no. 4, pp. 1193–1204, Dec. 2015.

[27] C. Zhang, X. Cai, and Z. Li, "Stability criterion and mechanisms analysis of electrical oscillations in the grid-tied VSC system," *Proc. CSEE*, vol. 37, no. 11, pp. 3174–3183, 2017.

[28] X. Chen, Y. Wang, and C. Gong, "Overview of stability research for grid-connected inverters based on impedance analysis method," *Proc. CSEE*, vol. 38, no. 7, pp. 2082–2094, 2018.

[29] C. Zhang, W. Wang, and G. He, "Analysis of sub-synchronous oscillation of full-converter wind farm based on sequence impedance and an optimized design method for PLL parameters," *Proc. CSEE*, vol. 37, no. 23, pp. 6757–6767, 2017.
[30] J. Lv, X. Cai, and Z. Zhang, "Impedance modeling and stability analysis of MMC-based HVDC for offshore wind farms," *Proc. CSEE*, vol. 36, no. 14, pp. 3771–3781, 2016.
[31] C. Zhang and X. Zhang, *PWM Rectifier and its Control*. Beijing, China: China Machine Press,2003.
[32] *IEEE Guide for Planning DC Links Terminating at AC Locations Having Low Short-Circuit Capacities*, Standard 1204–1997, Jan. 1997, pp. 1–216, doi: 10.1109/IEEESTD.1997.85949.
[33] S. Hu, *Principle of Automatic Control*. Beijing, China: Science Press, 2001.

FANG LIU (Senior Member, IEEE) received the B.S., M.S., and Ph.D. degrees in electrical engineering from the Hefei University of Technology, China, in 2005, 2008, and 2015, respectively. She is currently working as an Assistant Professor with the School of Electrical and Automation Engineering, Hefei University of Technology. Her current research interests include PV systems, energy storage systems, and control of microgrid systems.

LINFENG HU received the B.S. degree in electrical engineering from the Anhui University of Technology, China, in 2022. He is currently pursuing the M.S. degree in electrical engineering with the Hefei University of Technology, China. His current research interests include new energy grid-connected power generation and stability control.

GENGTAO YUAN received the B.S. degree in electrical engineering from the Shenyang University of Technology, China, in 2021. He is currently pursuing the M.S. degree in electrical engineering with the Hefei University of Technology, China. His current research interests include new energy grid-connected power generation and stability control.

BO LIU received the B.S. degree in electrical engineering from Wuhan Textile University, China, in 2022. He is currently pursuing the M.S. degree in electrical engineering with the Hefei University of Technology, China. His current research interests include new energy grid-connected power generation and stability control.

YUANYUAN BIAN received the B.S. degree in electrical engineering from the Shanghai University of Electric Power, China, in 2022. She is currently pursuing the M.S. degree in electrical engineering with the Hefei University of Technology, China. Her current research interests include new energy grid-connected power generation and stability control.